

Vibrational spectroscopy of fast-quenched ZrSiO_4 melts produced by laser treatments: local structures and decomposed phases

Ming Zhang^{1,5}, Ekhard K H Salje¹, Ai Hua Wang², Xiao Jia Li³,
Chang Sheng Xie², Simon A T Redfern¹ and Ren Xian Li⁴

¹ Department of Earth Sciences, University of Cambridge, Downing Street, Cambridge CB2 3EQ, UK

² State Key Lab of Plastic Forming Simulation and Die and Mould Technology, Department of Material Science and Engineering, Huazhong University of Science and Technology, Wuhan, 430074, People's Republic of China

³ Dalian Institute of Chemical Physics, Chinese Academy of Science, 457 Zhongshan Road, Dalian 116023, People's Republic of China

⁴ School of Mechanical Engineering, Southwest Jiaotong University, Chengdu 610031, Sichuan, People's Republic of China

E-mail: mz10001@esc.cam.ac.uk

Received 20 June 2005, in final form 16 August 2005

Published 30 September 2005

Online at stacks.iop.org/JPhysCM/17/6363

Abstract

Rapidly quenched ZrSiO_4 melts produced by CO_2 and pulsed YAG lasers have been analysed using infrared (IR) and Raman spectroscopy. The quenched melts exhibit decomposition into binary oxides (ZrO_2 and SiO_2), while other phases or complex SiO_4 tetrahedron networks are also observed. The local structures and the phases of the quenched melts depend strongly on the quenching rate and melting conditions. Monoclinic ZrO_2 are found to be the main ZrO_2 phase in the samples treated by CO_2 laser, although tetragonal ZrO_2 was found near boundaries between the untreated and melted regions. High concentrations of tetragonal ZrO_2 were detected in the samples treated by pulsed YAG lasers. Our observations indicate that the formation of tetragonal ZrO_2 is related to relatively high quench rates. Micro-IR and Raman data from areas near the boundaries between the quenched melts and untreated zircon show systematic variations of local structures and compositions. We observe a small region with relatively low density between the untreated and melted boundaries, which consists of tetragonal ZrO_2 or glassy ZrO_2 , and SiO_2 . Broad vibrational bands occur in the wavenumber region where the characteristic frequencies of zircon are located. This observation could indicate the possible existence of small amounts of glassy ZrSiO_4 in the melt state of zircon, although zircon tends to decompose above the melting point. These observations are in sharp contrast with the behaviour of radiation-damaged zircon, the so-called metamict zircon,

⁵ Author to whom any correspondence should be addressed.

where no phase separation occurs in samples which have not been subsequently annealed.

1. Introduction

Zircon, ZrSiO_4 , is a highly refractory material which is difficult to grow as single crystals but common in nature as natural minerals. Its great significance is due to the observation that zircon can incorporate radiogenic elements such as U, and Pu. Their radioactive decay leads to damage formation that is limited to areas next to the radiogenic nuclei. This observation leads to the idea to use zircon as host material for the immobilization and disposal of activity containing radioactive waste (Anderson *et al* 1993, Ewing *et al* 1995, Weber *et al* 1996). The nature of the radiation damage has been investigated in great detail (Murakami *et al* 1991, Ewing 1994, Weber *et al* 1998, Salje *et al* 1999, Ewing *et al* 2003). Experimental studies by NMR spectroscopy (Farnan and Salje 2001) and x-ray diffraction (Ríos and Salje 1999) have shown that the structural state of the radiation amorphized region depends explicitly on the radiation dose. This implies that the 'glassy' regions of such material cannot be equivalent to a thermal glass which would be the same for all materials. In fact, computer simulation by Trachenko *et al* (2002) showed that the damaged regions are highly structured with significant changes in density within each region. Such strong heterogeneities on an atomic length scale were also found using small angle scattering techniques by Ríos and Salje (2004). In a spectroscopic study, Zhang *et al* (2000a) raised the issue of whether the molten and radiation-damaged zircons have similar structural states.

In this study we compare, for the first time, phonon spectra of rapidly quenched zircon melts with those of radiation-damaged zircon. We will show that both materials are fundamentally different. Thermal glasses show phase separation even for the fastest quench while metamict materials show no such phase separation (unless they are thermally treated after the initial radiation damage).

We undertook the present investigation as a continuation of our recent series of Raman and infrared spectroscopic studies on amorphization and recrystallization of metamict zircon (Zhang *et al* 2000a, 2000b, 2000c). Our present study was also driven by the lack of understanding of the local structure and possible phases of fast-quenched thermal zircon melt. Although it has been reported that above ~ 2000 K zircon tends to decompose into its oxides (Butterman and Foster 1967) and simulations of amorphous zircon by melt quenching were recently reported (Devanathan *et al* 2004), there is a lack of detailed experimental investigations of the local structures of quenched ZrSiO_4 melts. In the present work, high-power laser techniques, which were commonly used for heating and melting (see, e.g., Wood and Giles 1981), were utilized to melt zircon for the following reasons. First, the melting temperature of ZrSiO_4 , above 2670 K (Butterman and Foster 1967), is too high to achieve for most common furnaces. Second, we wish, in some degree, to simulate the 'thermal spike', an ultra-fast heating and quenching process, which in a simple picture is considered to take place in the centre of cascades produced by alpha decay recoils (see, e.g., Miotello and Kelly 1997, Meldrum *et al* 1998), while more sophisticated computer simulation (Trachenko *et al* 2002) shows the stratification of this 'local melt'. It is of significance to gain understanding of the temperature and pressure associated with the process. We were, of course, aware of the fact that the quench time of radiation damage is only a few pico-seconds, which is much faster than the quench time in our laser heating experiments, in which the rates for the pulsed YAG laser treatment are in sub-milliseconds. Nevertheless, this quench time is faster than the time for thermal decomposition of metamict zircon at, say, ~ 1050 K (Zhang *et al* 2000a). We also wished to

Table 1. Chemical compositions of zircon samples studied.

	ZrO ₂	SiO ₂	FeO	HfO ₂	CaO	Al ₂ O ₃	Y ₂ O ₃	ThO ₂	UO ₂	Total
Crystal	65.41	31.37	—	1.28	0.01	0.01	0.01	0.01	0.02	98.34
	ZrO ₂	SiO ₂	Al ₂ O ₃	TiO ₂	Fe ₂ O ₃	CaO	Na ₂ O	MgO	K ₂ O	
Refractory	Balanced	29.90	4.00	0.30	0.25	0.48	0.02	0.20	0.04	
—undetectable										

explore the impact of melt quenching on its surrounding regions and the possible structural variations near the boundaries between the melted and untreated regions to gain understanding of the possible impact of melting and quenching on its surrounding regions.

2. Experimental methods

The starting materials were single crystals of natural zircon originating from Uganda and zircon refractory. The refractory sample showed a homogeneous microstructure with pores generated by the conventional refractory production. The untreated (containing Al and other trace elements, table 1) and the CO₂ treated refractory samples were previously studied by Wang *et al* (2004). Electron microprobe analysis (Cameca SX5D electron microprobe with a Link AN10000 energy-dispersive spectrometer, a beam size of 5 μm and beam current of 100 nA) showed that the crystal sample contained typical impurities of Hf, Ca, Al, Y, Th and U (table 1). X-ray Guinier powder diffraction measurements (with Si as internal standard) show that it has ideal cell parameters of $a = 6.6056$ and $c = 5.9834$ (Å), indicating its well crystallized structure. The CO₂ laser treatments (with a continuous wave and multimode, laser power of 1.5–2.0 kW) were carried out with beam sizes of 4 mm in diameter. The refractory was treated with a scanning velocity of 4–16 mm s⁻¹, whereas the crystal samples were irradiated for 1, 3 and 5 s. The CO₂ laser-treated refractors have relatively smooth surfaces as shown by Wang *et al* (2004). Overlapping treatments were also done for the refractory samples with an overlapping ratio of 25%. This produced regions double scanned by the laser. The laser treated regions show bulbs with sizes ranging from a few micrometres up to several hundred micrometres in both refractory and crystal samples. The pulsed YAG-laser treatment was done with power of 95–500 W, pulse widths of 0.3 and 0.5 ms and repetition frequency of 30 and 60 Hz. Data were recorded from those areas that are free of bulbs. We noted that all treated surfaces became white. This is likely to be the direct result of decomposition of zircon into ZrO₂ and SiO₂, as a similar colour change has been noted in thermally decomposed metamict zircon in our previous high-temperature experiments (Zhang *et al* 2000a, 2000b).

The infrared powder pellet technique reported by Zhang *et al* (1996) was used for powder absorption measurements. Polyethylene and CsI were used as matrix materials for the far infrared measurements, whereas KBr was used for the measurements in the mid-infrared region. Sample/matrix ratios are 1:50, 1:300 and 1:400 for polyethylene, CsI and KBr, respectively. Sample powders were thoroughly mixed with the matrix materials. A few drops of pentane were used for the mixing of the sample and polyethylene powder to reduce static charges caused by the mixing. The mixtures were pressed into 13 mm discs under vacuum. The sample pellets were used within 12 h of preparation.

Two infrared spectrometers were used to record the IR data. The reflectance measurements were recorded with a Bruker IFS 113v spectrometer equipped with an IRscope-II infrared microscope. A liquid-nitrogen-cooled MCT detector was chosen to couple with a Globar source and a KBr beamsplitter. Micro-IR reflectance data in the mid-IR region were collected

for CO₂- or YAG-laser-treated samples using a microscope with a 36× objective and a beam size of 20 μm. Conventional specular reflectance spectra in 50–5000 cm⁻¹ were recorded for an untreated single crystal and CO₂-laser-treated samples at close-to-normal incidence conditions using a Bruker reflectance accessory. Gold mirrors were used as references. IR powder absorption spectra were recorded using a Bruker IFS 66v spectrometer. The spectra were measured in two separate regions: (1) 50–500 cm⁻¹ (with polyethylene and CsI pellets, a DTGS detector with a polyethylene window, a 3.5 μm Mylar beamsplitter and a Globar lamp) and (2) 350–5000 cm⁻¹ (with KBr pellets, a MCT detector, a KBr beamsplitter and a Globar lamp). The IR spectra were obtained over 350–3500 scans with an instrumental resolution of 2 cm⁻¹.

Micro-Raman data were collected with a free-sample-space LabRam micro-Raman spectrometer and a Renishaw Raman microscope (Ramascope-1000). Three lasers (623.8, 532.2 and 514.5 nm) were used for the excitation. CCD detectors, a grating (1800 or 1200 grooves/mm), a 50× ultra-long working distance and a 100× objective were adapted. In order to check any possible laser-induced fluorescence, FT-Raman spectra were also recorded at room temperature using a Bruker FRA 106 FT-Raman accessory attached to the Bruker IFS 66v spectrometer. A silicon-coated calcium fluoride beam-splitter and radiation of 1064 nm from a Nd:YAG laser were used for the excitation laser and the focused beam was about 200 μm in size. A liquid-nitrogen-cooled, high sensitivity Ge detector was used, and the spectra with resolution of 2 cm⁻¹ were recorded with a laser power of 45–100 mW and a back scattering geometry.

3. Results

3.1. IR spectra of quenched ZrSiO₄ melts

Zircon (ZrSiO₄) is tetragonal with space group D_{4h}¹⁹ or I4₁/amd and Z = 4. Group theory (Dawson *et al* 1971) predicts seven IR-active normal modes (3A_u + 4E_u) and 12 Raman-active modes (2A_{1g} + 4B_{1g} + B_{2g} + 5E_g) in zircon at *k* = 0. The IR and Raman bands can be classified into two vibration groups, internal bands of SiO₄ tetrahedra and external bands associated with the Zr motions, the rotations and translations of the SiO₄ tetrahedra. The former is mainly located between 500 and 1100 cm⁻¹ and the latter in the far infrared region.

The laser-treated samples show spectral features different from untreated samples (figure 1). The CO₂-laser-treated samples show relatively sharp bands between 120 and 800 cm⁻¹ and broad features between 800 and 1300 cm⁻¹, in contrast to the untreated sample. The presence of these bands in the far IR region shows the decomposition of zircon, as their band positions agree with these of monoclinic ZrO₂ (m-ZrO₂) and glassy SiO₂. This finding is further confirmed by reflectance measurements on the quenched melts (figures 2(a)–(c)). The persistence of absorption features near 320 and 900 cm⁻¹, whose frequencies are consistent with bands of zircon, suggests that small amounts of zircon or materials with Si–O bonding similar to those in zircon probably coexist with the ZrO₂ and SiO₂ in the quenched melts. This is further confirmed by Raman measurements.

Micro-IR measurements (with a beam size of 20 μm) were carried out to explore the local configurations of the treated refractory samples, which have relatively large and flat surfaces, as well as the degree of the heterogeneities. The analysis shows that in respect to the beam size used, most of the CO₂-laser-melted regions have essentially similar spectral patterns, indicating a similar local structure. However, systematic changes of spectral features were found to occur near the edges or boundaries between melted and untreated regions (figure 3(a)) as well as near those between the single-scanned and double-scanned regions (the double-scanned regions are

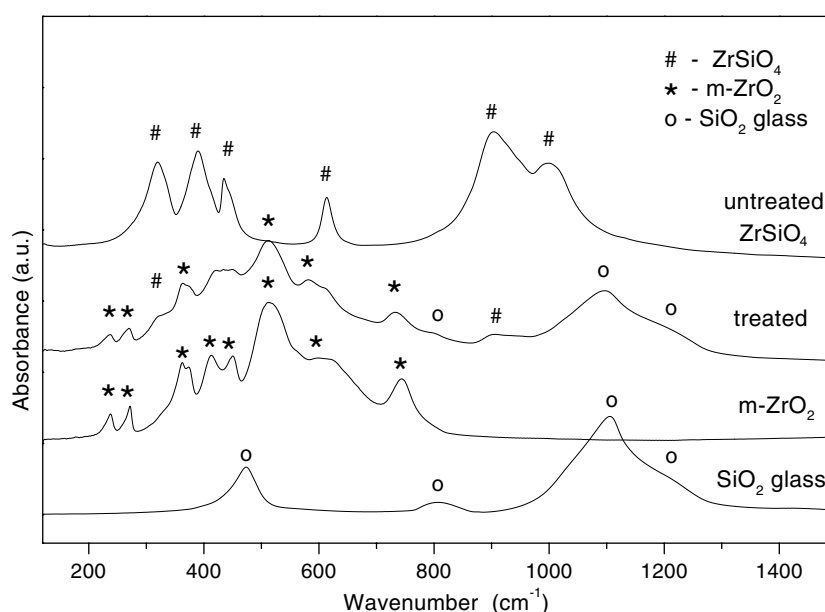


Figure 1. Comparisons of IR powder absorption spectra of untreated and CO₂-laser-treated sample, and monoclinic ZrO₂ and SiO₂ glass.

formed as a result of the overlapping treatments with overlapping ratio of 25%; and more details can be found in Wang *et al.* (2004) (figure 3(b)). The distance indicated in figures 3(a) and (b) represents the location of the measured area from the edges. One of the interesting observations from our micro-IR data is the systematic change of the spectral pattern (figures 3(a) and (b)) and the significant decrease in reflectivity (from 0.8 to 0.2) and peak frequency (from 1120 to 1076 cm⁻¹, directly measured from reflectance data) of the main Si–O stretching band (figures 4(a) and (b)) when the sampled areas move from the melts to its untreated–treated boundaries. The variation is expected to be associated with changes of the local configurations (Mochizuki and Kawai 1972). The micro-IR data on CO₂-laser-treated samples also show that the intensity of m-ZrO₂ depends on the sampled areas. Near the edge between the untreated and molten regions, the 731 cm⁻¹ band of the m-ZrO₂ phase can be hardly detected. However, this band becomes more and more intense when the sampled areas move away from the edge. The lack of m-ZrO₂ signals in the edge suggest that as a result of the decomposition of ZrSiO₄ other ZrO₂ phases (e.g., glassy, tetragonal, even cubic ZrO₂) or other unknown phases must exist. Unfortunately, IR bands of tetragonal and cubic ZrO₂ are located in the far IR region, which is out of the detection range of the micro-IR measurements. However, the existence of tetragonal ZrO₂ (t-ZrO₂) near the boundaries is further confirmed by Raman measurements (see below).

The YAG laser treatment was carried out only for the natural zircon single crystals. The treatment (with a pulse width of 0.3 ms) results in the formation of a thin layer (a few micrometres) of melts on the crystal surface. Micro-IR data (with a beam size of 20 μm) were randomly recorded from a melted area of 2 × 2 mm². The IR data show a variation of spectral features, in contrast to CO₂-laser treated samples that show generally similar IR patterns in most regions (except the treated and untreated boundaries). Some of the typical features of the YAG-laser-treated samples are shown in figure 5. The features between 800 and 1200 cm⁻¹ are mainly associated with vibrations from the SiO₄ tetrahedra. The reflectivity and general

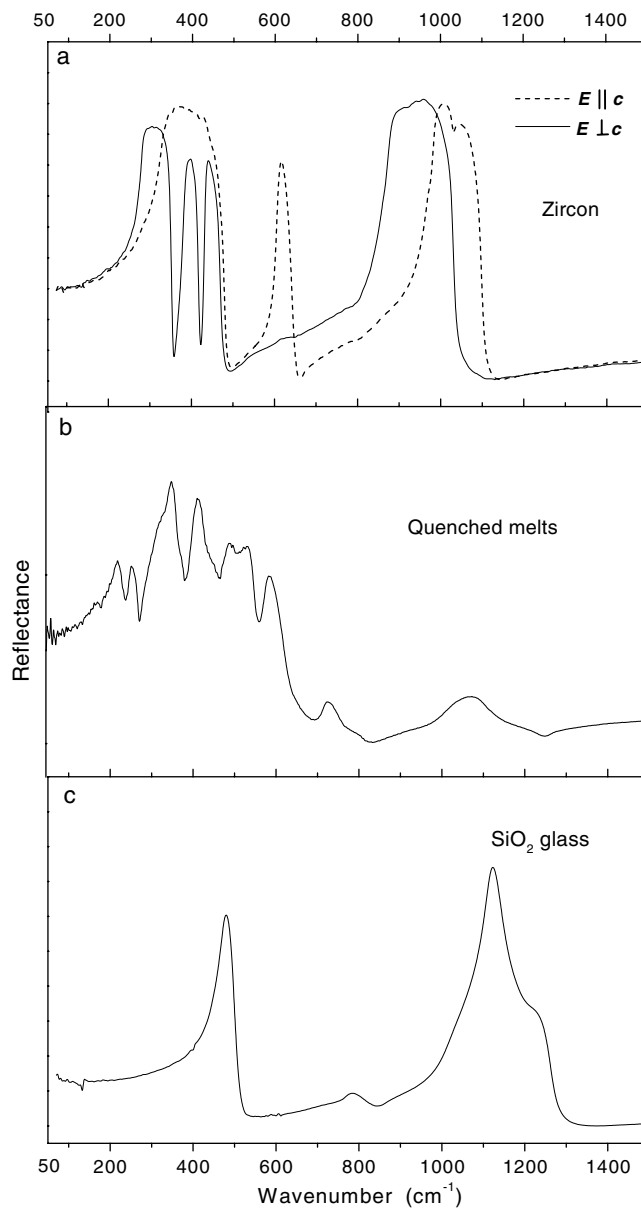


Figure 2. IR reflectance spectrum between 50 and 1500 cm^{-1} : (a) zircon; (b) CO_2 -laser-treated sample; and (c) SiO_2 glass.

shape, which vary from area to area, indicate the existence of various local configurations related to SiO_4 within the scale of the beam size used ($\approx 20 \mu\text{m}$).

3.2. Raman spectra of quenched ZrSiO_4 melts

Micro-Raman spectroscopy was used to characterize the structural change caused by the two laser treatments, and the effects of the CO_2 - and YAG-laser treatments are described here

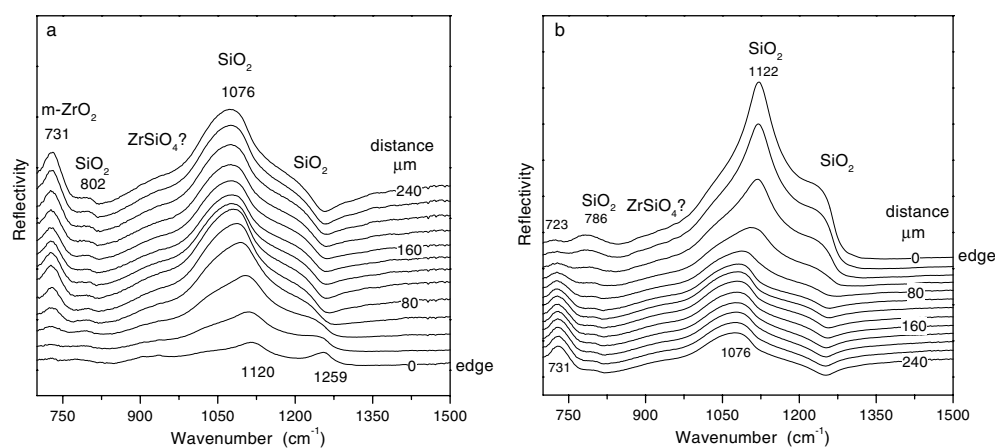


Figure 3. Micro-IR reflectance spectra from areas (a) near the boundary between untreated and treated regions of refractory sample and (b) near the overlay regions. Please note that the spectra recorded near the edges are placed at the bottom in (a), whereas they are at the top in (b) for an easy stack plot.

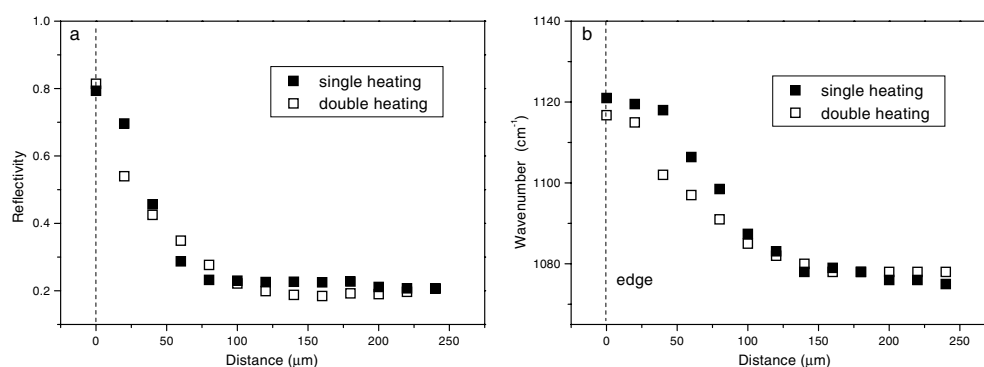


Figure 4. Reflectance (a) and position (b) of the feature near 1100 cm^{-1} as a function of distance from the edge.

separately. The CO₂-laser-treated zircon crystals and refractory show sharp and intense signals of m-ZrO₂ (figure 6), consistent with the observations of the IR measurements. The Raman bands of the co-existing SiO₂ glass, as previously seen in the IR data, could hardly be resolved, probably because of their overlap with strong m-ZrO₂ bands and its weak Raman intensity associated with the amorphous structures. This indicates that ZrO₂ is better resolved in Raman spectra. We also noted that increasing irradiation time and power generally leads to relatively large ZrO₂ gains. Micro-Raman mapping measurements (with a beam size of $\sim 1\ \mu\text{m}$ and a step of $1\ \mu\text{m}$) were carried out near the boundaries between the untreated and melted regions as to further investigate the variation of local structures as revealed by IR. The analysis shows that on approaching the boundaries different phases commonly exist with a general pattern—a change from pure zircon (ZrSiO₄), to t-ZrO₂ and then m-ZrO₂, although t-ZrO₂ did not appear in all boundaries.

The laser treatment seems to have no or little effect on the frequencies of Raman bands of the remaining zircon domains. For example, the 976 cm^{-1} (stretching vibration of SiO₄) and 1008 cm^{-1} (Ag, stretching vibration of SiO₄) bands of zircon, which are due to stretching

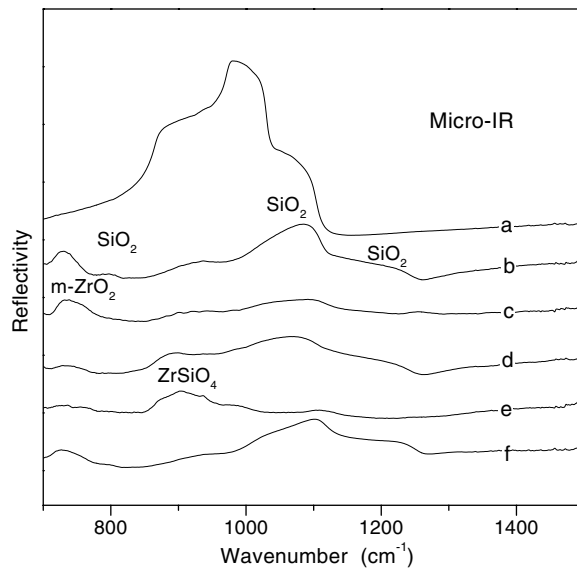


Figure 5. Typical unpolarized micro-IR spectra of pulsed YAG-laser treated crystals (pulse width of 0.3 ms). Spectrum (a) is recorded from untreated zircon, and spectra (b)–(f) are obtained from treated regions. The variety of spectral features in spectra (b)–(f) indicates the structural variations in the different sampled areas.

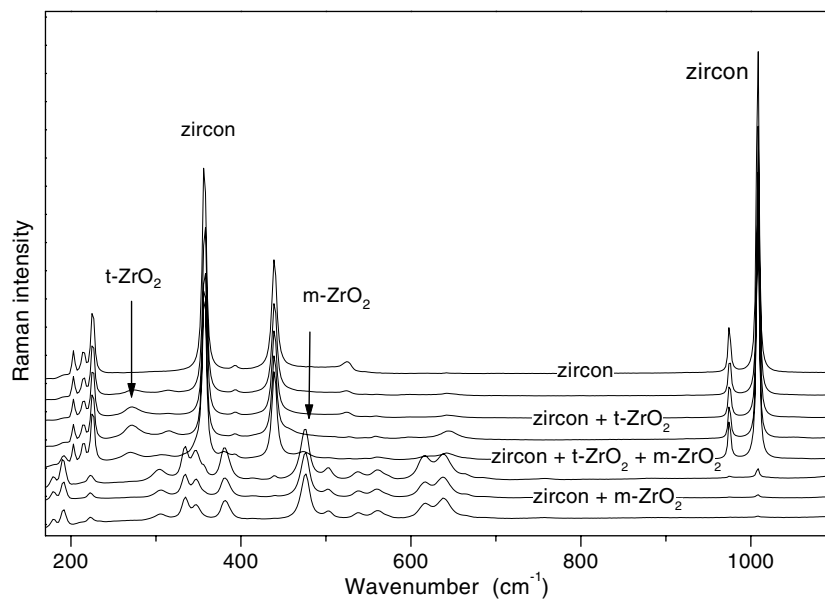


Figure 6. Micro-Raman spectra of natural zircon crystal treated by CO₂ lasers. The data are recorded from a length of 30 μm in the boundaries.

vibrations of SiO₄, show no detectable change in frequency when measured from the untreated regions to the melted regions. Interestingly, broad signals near 976 and 1008 cm⁻¹ were also recorded in some areas of the CO₂ laser-treated samples (figure 7). The frequencies

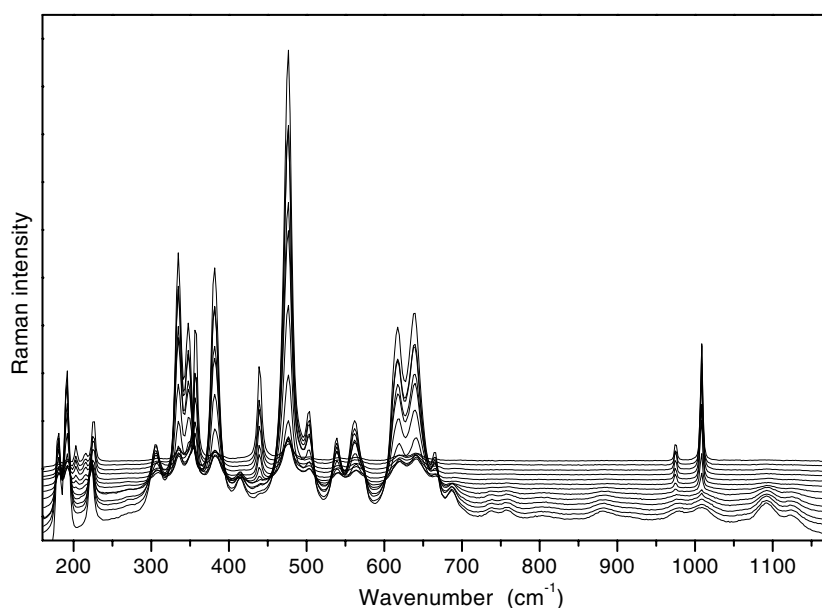


Figure 7. Micro-Raman spectra of the CO₂-laser-treated crystal. The data were obtained by the Raman mapping method along a length of 12 μm .

are essentially identical to these of stretching vibrations of SiO₄ in zircon. However, these bands recorded in the melt regions have measured bandwidths of $\sim 25\text{ cm}^{-1}$, in contrast to width values of $3\text{--}4\text{ cm}^{-1}$ in the untreated samples. As SiO₂ glasses and ZrO₂ phases do not have characteristic Raman bands in these wavenumbers, these broad bands could suggest the formation of amorphous phases, or laser-induced luminescence bands. FT-Raman measurements were carried out in the treated crystals and refractory for further confirmation. The FT-Raman data show a broad feature between 900 and 1200 cm^{-1} . The feature is located in a similar frequency region as these broad features, 976 and 1008 cm^{-1} , although its general shape is less resolved in comparison to those spectra obtained by micro-Raman analysis, which is well known to have a much higher sensitivity. The slightly different features between 900 and 1200 cm^{-1} in the FT-Raman (with beam sizes of $\sim 200\text{ }\mu\text{m}$) and conventional micro-Raman (beam sizes of a few micrometres) results could also be due to the fact that the FT-Raman measurements were averaged over large regions. The observations suggest that apart from decomposition into ZrO₂ and SiO₂, quenched ZrSiO₄ melts contain small amounts of disordered or amorphous domains of ZrSiO₄ glass, i.e., disordered phases with SiO₄ connected somewhat similarly as those in zircon. The effect of scanning speed on the final phases of the treated samples is not very significant in terms of Raman spectroscopy, but the Raman intensity changes and ZrO₂ phases become more detectable at low scanning rates.

T-ZrO₂ and m-ZrO₂ grains were detected in the YAG-laser-treated sample. The former appeared in almost all treated sample areas, in contrast to its main presences near the boundaries in CO₂-laser-treated samples. This finding indicates that the t-ZrO₂ phase has a higher concentration in the YAG-laser-treated samples. Under optical microscopes, the t-ZrO₂ grains look transparent, whereas m-ZrO₂ grains are essentially white. The micro-Raman data on YAG-laser-treated samples reveal, apart from the characteristic bands of t- and m-ZrO₂, additional spectral patterns: broad features in the region of between 150 and 700 cm^{-1} , where bands of ZrO₂ are commonly located (figure 8). Detailed analysis implies that these features

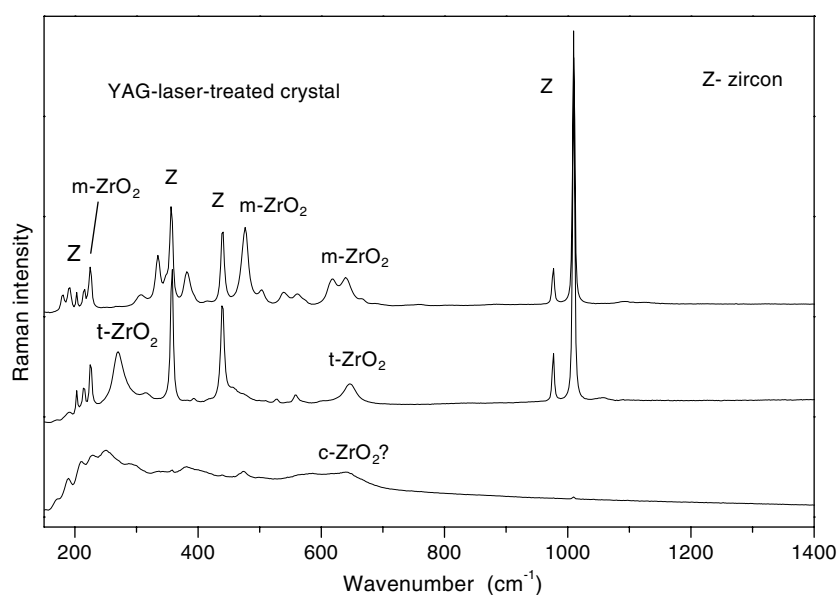


Figure 8. Typical micro-Raman spectra of YAG-laser-treated crystals (pulse width of 0.3 ms). Different ZrO_2 phases are revealed. The shape of the bottom spectrum is similar to that of cubic ZrO_2 .

tend to appear near the boundaries between the melted and the untreated regions (figure 9). We suspect that these features are due to cubic or glassy ZrO_2 . Most interestingly, these broad features are not recorded or revealed in the CO_2 -laser-treated samples. The differences are expected to be due to different quench rates between the CO_2 - and YAG-laser treatments.

4. Discussion

Laser melting and quench in air leads to decomposition of zircon into SiO_2 and ZrO_2 . This result is in contrast to the behaviour of amorphous phase(s) produced by alpha-decay damage in zircon (e.g., Murakami *et al* 1991, Zhang *et al* 2000c, Farnan and Salje 2001). The Raman and IR data on laser-treated zircon show spectra different from those of highly metamict zircon reported by Zhang *et al* (2000a, 2000b). The differences are mainly in two aspects. First, the decomposition of ZrSiO_4 into ZrO_2 and SiO_2 occurs only in thermally heated samples, while highly metamict zircon crystals reported in previous studies remain undecomposed. In thermal glass, the SiO_4 tetrahedra in SiO_2 are linked in such a way as to form a ring structure, which contributes vibrational features near 1100 cm^{-1} (figures 3(a) and (b)). In SiO_2 , each oxygen atom is connected to two Si atoms, in a state known as full polymerization. In contrast, the spectra of metamict zircon show very broad features between 800 and 1000 cm^{-1} (Zhang *et al* 2000c). As band frequency is directly related to bond strength and local configuration, these frequency differences between the two types of materials indicate variations in Si–O banding and Si–O–Si linkages. This observation is in agreement with those of Farnan and Salje (2001). Second, the laser treatments have weak effect on the frequency of the vibrational modes associated with the remaining domains of ZrSiO_4 , in contrast to those in self-radiation-damaged natural zircon (Nasdala *et al* 1995, Zhang *et al* 2000c, Geisler *et al* 2001). We observed that the Raman band near 1008 cm^{-1} (stretching vibration of SiO_4) of zircon showed

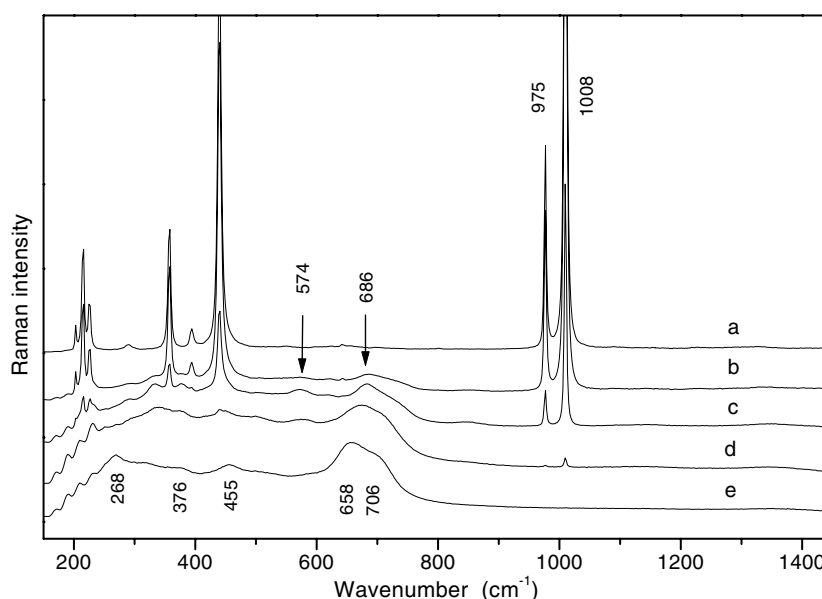


Figure 9. Broad Raman features were recorded near the boundaries (spectrum a is obtained from untreated zircon near the boundary, whereas spectrum e is indicative of an amorphous-type phase; data in (b)–(d) show the mixtures of these phases). The data are recorded along a length of 10 μm from YAG-laser treated crystals.

no significant change in frequency in CO₂- and YAG-laser-treated samples, although it became significantly broader. This means that some ZrSiO₄ remains within the initial sample without being significantly altered.

The results from the present work also show that the final phases in the quenched melts can be strongly affected by the quench rate. Pure zirconia exists in different crystalline structures at different temperatures and pressures (Smith and Newkirk 1965). At room temperature, it has a monoclinic structure (space group $P2_1/c$). On heating, m-ZrO₂ undergoes a phase transition into a tetragonal structure ($P4_2/nmc$) near 1170 °C. On further heating it transforms into cubic ZrO₂ ($Fm\bar{3}m$) near 2370 °C. Two orthorhombic zirconia phases can also form by cooling Mg-stabilized ZrO₂ and by quenching ZrO₂ powder from 600 °C and 6 GPa (Howard *et al* 1991). ZrO₂ exists as melts above 2680 ± 15 °C (Latta *et al* 1970). Our data show that the presence of monoclinic and tetragonal ZrO₂ dominates the decomposed materials. Cubic ZrO₂ might also exist in the quenched melts. As the single crystals used in this present study do not contain significant chemical impurities, which could stabilize the tetragonal and cubic phases (high temperature phases), the appearance of these different phases may relate to the quench rate or/and local strains. Although the melted regions produced by CO₂ laser treatments generally show similar spectral patterns indicative of essentially similar phases, the systematic change of SiO₄ spectra and the appearance of t-ZrO₂ near the boundaries between the untreated and melted regions indicate a variation of the local structure. The main cause for this spectral difference between the boundaries and other melted regions is associated with melting conditions and quenching rates. It is presumed that there is a larger temperature gradient near the boundaries, and the area has a cooling rate higher than those in the other melted regions. With higher cooling rates, higher temperature phases or structures are more likely to be preserved or 'frozen' during quenching. As a result, t-, c-ZrO₂, even glassy ZrO₂

may form. This conclusion is further supported by the results from YAG-laser-treated samples, which show significant amounts of t-ZrO₂, together with cubic-like and amorphous-like ZrO₂. As the YAG laser treatment (with pulse widths of 0.3 and 0.5 ms) involves higher heating and quenching rates in comparing with CO₂ laser treatments (the irradiation times are in the order of seconds), therefore the melting and quenching process is faster than that produced by CO₂ laser treatments. This explains why the YAG-laser-treated samples have relatively high contents of t-ZrO₂ with respect to the CO₂-laser-treated samples.

Information on the local configurations associated with the linkage of SiO₄ groups in the melts can be further extracted by examining its peak profiles. Raman features of SiO₂ glass have been used to identify its defects and local structures (e.g., Geissberger and Galeener 1983, Pasquarello and Car 1998), but we were unable to resolve the Raman bands of SiO₂ because of their weak Raman intensity and their overlapping with very strong m-ZrO₂ bands. As a result, we used a strong IR band of SiO₂ to explore its local structure. The IR feature near 1100 cm⁻¹ in quenched melts is associated with the asymmetric stretching in the SiO₄. It has been generally accepted that the basic SiO₄ tetrahedral building blocks are linked with some bridging (Si–O–Si) bonds to form ring structures. According to the central force ideal continuous random network model, the frequency value of the 1100 cm⁻¹ IR band is proportional to the squared root of the cosine of the Si–O–Si bridging bond angle (Hosono 1991). Devine (1993) suggested that the increase in the band frequency from 1030 to 1110 cm⁻¹ was associated with a change in the angle from 130° to 160° and eventually saturated near 180°. The peak position of this IR band is also related to its oscillator strength (Awazu 1999). We noted that in comparison with neutron and ion implanted amorphous SiO₂ (Devine 1993) our observed frequency (1075–1120 cm⁻¹) of the IR asymmetric stretching in the SiO₄ is apparently higher than those (1037–1080 cm⁻¹) of the implanted materials (Devine 1993). It is interesting that although the IR spectral patterns of SiO₂ recorded in the regions far from the edges are different from those implanted SiO₂ (Herrmann *et al* 1996), the data recorded near the boundaries between the untreated and melted regions show features (between 900 and 1200 cm⁻¹) similar to that reported in ion implanted SiO₂ (Hosono 1991, Herrmann *et al* 1996).

Tan *et al* (1998) have suggested a relationship between the frequency of the strong Si–O stretching band near 1100 cm⁻¹ and the local density of SiO₂ glass. The IR data recorded near the edges show similar spectral patterns and frequencies to those with density of 2.20 g cm⁻³ reported by Tan *et al* (1998). With the calibrations of Tan *et al* (1998), the density variation associated with SiO₂ in our laser treated samples is estimated to be between 2.20 and 2.71 g cm⁻³. It increases from the edge to the melted region. This finding suggests that the SiO₄ tetrahedra are less densely compacted near the boundaries in comparison to the other melted regions. Unfortunately, we were unable to measure or estimate the overall density of the quenched ZrSiO₄ melts, because the material (obtained from both zircon crystals and refractory) contains bubbles which would strongly affect the outcome of the density measurement. The non-uniform distributions of the tetragonal, monoclinic ZrO₂ and glass-like ZrSiO₄ make it difficult to extract their portions and further complex the determination of the real value of overall density in the region, but a quantitative estimation could be drawn with considering the quenched melts containing SiO₂ and ZrO₂. It has been reported that the density of ZrO₂ changes with its crystal structures (density ratio c-ZrO₂:t-ZrO₂:m-ZrO₂ = 1.00:1.02:1.07) (French *et al* 1994). As more t- or c-ZrO₂ grains (with relatively low density in comparison to m-ZrO₂) are observed near the boundaries and the SiO₂ phase in the region also has a low density (about 2.20 g cm⁻³), it is fair to conclude that the boundaries have lower density values relative to the melts. The observation of the formation of bubbles in quenched melts is consistent with the fact that melting leads to a dramatic increase in the volume of zircon and fast quenching results in a sudden decrease in

volume. A recent molecular dynamic simulation (Devanathan *et al* 2004) indicates a dramatic increase (the value is nearly doubled) in the molar volume of zircon at the melting point. We believe that the formation of the bubbles is the consequence of the sudden decrease in the volume of the melts on fast quenching.

We now discuss the formation of tetragonal and monoclinic ZrO₂ in the quenched melts of ZrSiO₄. Although both phases appeared in both YAG- and CO₂-laser-treated samples, the tetragonal phase appeared only in limited regions, mainly near the boundaries. In contrast, the tetragonal phase was recorded in most regions in YAG-laser-treated samples, in which the quench rate is much higher. Based on these observations, we think that the formation of tetragonal ZrO₂ is the direct results of a faster quench process, whereas monoclinic ZrO₂ finally forms with lower quench rate. The relatively low values of the ZrO₂ bands could be an indication of their small crystalline size.

5. Conclusions

The IR and Raman data obtained in the present study show that the ZrSiO₄ material produced by laser melting and quenching consists of crystalline (also possible amorphous) ZrO₂ and glassy SiO₂, together with some zircon domains. The local structures of the decomposed phases are strongly affected by the melting and quenching conditions. Fast quenching tends to produce more tetragonal ZrO₂, or even cubic and amorphous phases. The observation of the broad bands near 976 and 1008 cm⁻¹ in ZrSiO₄ quenched melts could suggest the formation of a glass phase or an amorphous material with SiO₄ connected somewhat similarly as those in zircon. Our results indicate that in terms of fundamental structures radiation-induced aperiodic (metamict) zircon is different from ZrSiO₄ glasses quenched from melts.

Acknowledgments

Funding from British Nuclear Fuel Limited (BNFL), the Royal Society and the Cambridge-MIT Institute (CMI) is gratefully acknowledged. AHW and CSX thank the Fund of the Hubei Province Key Laboratory of Ceramic and Refractories, Wuhan University of Science and Technology, for the financial support.

References

- Anderson E B, Burakov B E and Vasiliev V G 1993 *Proc. Safe Waste 93* vol 2, p 29
- Awazu K 1999 *J. Non-Cryst. Solids* **260** 242
- Butterman W and Foster W R 1967 *Am. Mineral.* **52** 880
- Dawson P, Hargreave M M and Wilkinson G F 1971 *J. Phys. C: Solid State Phys.* **4** 240
- Devanathan R, Corrales L R, Weber W J, Chartier A and Meis C 2004 *Phys. Rev. B* **69** 064115
- Devine R A B 1993 *J. Non-Cryst. Solids* **152** 50
- Ewing R C 1994 *Nucl. Instrum. Methods Phys. Res. B* **91** 22
- Ewing R C, Lutze W and Weber W J 1995 *J. Mater. Res.* **10** 243
- Ewing R C, Meldrum A, Wang L M, Weber W J and Corrales L R 2003 *Rev. Mineral. Geochem.* **53** 387
- Farnan I and Salje E K H 2001 *J. Appl. Phys.* **89** 2084
- French R H, Glass S J, Ohuchi F S, Xu Y-N and Ching W Y 1994 *Phys. Rev. B* **49** 5133
- Geisler T, Pidgeon R T, van Bronswijk W and Pleysier R 2001 *Eur. J. Mineral.* **13** 163
- Geissberger A E and Galeener F L 1983 *Phys. Rev. B* **28** 3266
- Herrmann U, Dunker H H, Wendler E and Wesch W 1996 *J. Non-Cryst. Solids* **204** 73
- Hosono H 1991 *J. Appl. Phys.* **69** 8079
- Howard C J, Kisi E H and Ohtaka O 1991 *J. Am. Ceram. Soc.* **74** 2321
- Latta R E, Duderstadt E C and Fryxell R E 1970 *J. Nucl. Mater.* **35** 345

- Meldrum A, Zinkle S J, Boatner L A and Ewing R C 1998 *Nature* **395** 56
- Miotello A and Kelly R 1997 *Nucl. Instrum. Methods Phys. Res. B* **122** 458
- Mochizuki S-S and Kawai N 1972 *Solid State Commun.* **11** 763
- Murakami T, Chakoumakos B C, Ewing R C, Lumpkin G R and Weber W J 1991 *Am. Mineral.* **76** 1510
- Nasdala L, Irmer G and Wolf D 1995 *Eur. J. Mineral.* **7** 471
- Pasquarello A and Car R 1998 *Phys. Rev. Lett.* **80** 5145
- Ríos S and Salje E K H 1999 *J. Phys.: Condens. Matter* **11** 8947
- Ríos S and Salje E K H 2004 *Appl. Phys. Lett.* **84** 2061
- Salje E K H, Chrosch J and Ewing R C 1999 *Am. Mineral.* **84** 1107
- Smith D K and Newkirk H K 1965 *Acta Crystallogr.* **18** 982
- Tan C Z, Arndt J and Xie H S 1998 *Physica B* **252** 28
- Trachenko K, Dove M T and Salje E K H 2002 *Phys. Rev. B* **65** 18102(R)
- Wang A H, Wang W Y, Xie C S, Song W L and Zeng D W 2004 *Appl. Surf. Sci.* **227** 104
- Weber W J, Ewing R C, Catlow C R A, de la Rubia T D, Hobbs L W, Kinoshita C, Matzke H, Motta A T, Nastasi M, Salje E H K, Vance E R and Zinkle S J 1998 *J. Mater. Res.* **13** 1434
- Weber W J, Ewing R C and Lutze W 1996 *Mater. Res. Soc. Symp. Proc.* **412** 25
- Wood R F and Giles G E 1981 *Phys. Rev. B* **23** 2923
- Zhang M, Salje E K H, Capitani G C, Leroux H, Clark A M and Schlüter J 2000a *J. Phys.: Condens. Matter* **12** 3131
- Zhang M, Salje E K H, Ewing R C, Farnan I, Ríos S, Schlüter J and Leggo P 2000b *J. Phys.: Condens. Matter* **12** 5189
- Zhang M, Salje E K H, Farnan I, Graem-Barber A, Danial P, Ewing R C, Clark A M and Leroux H 2000c *J. Phys.: Condens. Matter* **12** 1915
- Zhang M, Wruck B, Graeme-Barber A, Salje E K H and Carpenter M A 1996 *Am. Mineral.* **81** 92